

Fast multiple inversion for stress analysis from fault-slip data

Katsushi Sato^{a,*}

^a*Division of Earth and Planetary Sciences, Kyoto University, Kyoto 606-8502, Japan*

Abstract

The multiple inverse method is widely used to invert multiple stress tensors from fault-slip data caused by polyphase tectonics. A practical problem of the method is the time-consuming computation related to its iterative procedure. This paper describes a way of accelerating the computation by replacing an exhaustive grid search for the optimal stress tensor by direct calculation using an analytical solution. Furthermore, a technique to reduce noise in the result was developed based on the estimation of instabilities of solutions.

Keywords: stress tensor inversion, tectonic stress, algorithm, even-determined problem, deviatoric stress space

1. Introduction

2 Stress tensor inversion methods are widely used to infer tectonic stress
3 state from fault-slip data. Input fault data are collected from geological out-
4 crops, seismic focal mechanisms, rock core samples and underground images
5 obtained by three-dimensional seismic surveys. Among the variety of meth-

*Corresponding author.

Email address: `k_sato@kueps.kyoto-u.ac.jp` (Katsushi Sato)

6 ods the multiple inverse method (Yamaji, 2000), hereafter abbreviated as
7 MIM, has an advantage in separating multiple stress tensors from a mix-
8 ture of geological faults yielded from spatial or temporal change of tectonic
9 stress state. This method has been used by many researchers in various
10 regions (e.g., Yamada and Yamaji, 2002; Yamaji, 2003; Sippel et al., 2009;
11 Chan et al., 2010) and further methodological improvement is now ongoing.
12 MIM has been extended to analyse seismic focal mechanisms without a pri-
13 ori specification of fault planes from paired orthogonal nodal planes (Otsubo
14 et al., 2008), improved to objectively recognise multiple solutions by means of
15 clustering techniques (Otsubo and Yamaji, 2006) and enhanced in its resolu-
16 tion through development of uniform computational grid (Sato and Yamaji,
17 2006b; Yamaji and Sato, 2011).

18 A fault-slip data set is described as heterogeneous when it includes faults
19 caused by different stresses. A conventional method of stress inversion (e.g.,
20 Angelier, 1979) determines an optimal stress tensor for a whole data set,
21 though the solution is meaningless if the data set is heterogeneous. MIM
22 can detect multiple stress tensors through an iterative sampling procedure.
23 When a data set has N faults, MIM extracts a subset including k faults from
24 it and determines an optimal stress tensor for the subset by exhaustive grid
25 search. This process is repeated ${}_N C_k$ times for all possible combinations of
26 k -element subsets. A great number of stress tensors are obtained and their
27 concentrations are interpreted as desired tectonic stresses (Fig. 1). This
28 iterative calculation also has an effect of enhancing solutions from natural
29 noisy fault-slip data.

30 A problem of MIM lies in its computational cost. It takes between a few

31 hours and several days to analyse several hundred to a thousand faults by a
32 personal computer. The cost is proportional to the number of fault subsets
33 ${}_N C_k$, which is order of $O(N^k)$ by Landau's symbol. The number of faults in
34 a subset k is empirically set to four or five (Yamaji, 2000). Therefore the cost
35 is $O(N^4)$ or $O(N^5)$. This fact generally limits the total number of faults N
36 up to a thousand.

37 Each determination of optimal stress for fault subsets is done by exhaus-
38 tive grid search on 60,000 uniformly spaced stress tensors (Sato and Yamaji,
39 2006b) by default. This study proposes a direct algorithm for determination
40 of optimal stress tensor. Although the new technique is applicable only to
41 four-element subsets, it calculates the numerous stress solutions several times
42 faster than conventional MIM. A method of noise reduction by estimating
43 instabilities of solutions is also provided.

44 **2. Method**

45 *2.1. Wallace-Bott hypothesis*

46 MIM as well as recent stress tensor inversion techniques is based on an
47 assumption that a fault slips in the direction of shear stress, which is called
48 Wallace-Bott hypothesis (Wallace, 1951; Bott, 1959, illustrated in Fig. 2a).
49 Input data of stress inversion analysis are called fault-slip data which contain
50 fault plane orientations, slip orientations and shear senses, while the unknown
51 parameters are described by stress tensors. The direction of shear stress on
52 a fault plane depends on four of the six independent components of stress
53 tensor. Let $\boldsymbol{\sigma}$, whose components are denoted by σ_{ij} ($i = 1$ to 3 , $j = 1$ to 3),
54 be a reduced stress tensor with four degrees of freedom. Two normalisation

55 conditions imposed on $\boldsymbol{\sigma}$ can be freely chosen. The first and second invariants
 56 are normalised in this study, i.e.,

$$J_1 = \sigma_1 + \sigma_2 + \sigma_3 = 0 \quad (1)$$

57 and

$$J_2 = -\sigma_1\sigma_2 - \sigma_2\sigma_3 - \sigma_3\sigma_1 = 1, \quad (2)$$

58 where σ_1 , σ_2 and σ_3 are the principal stress magnitudes ($\sigma_1 \geq \sigma_2 \geq \sigma_3$,
 59 compression is positive). Let $\mathbf{n} = (n_1, n_2, n_3)^T$ and $\mathbf{v} = (v_1, v_2, v_3)^T$ be the
 60 unit vectors in the directions of fault normal and slip direction, respectively.
 61 The superscript T denotes the transpose of a vector or a matrix. Hereafter
 62 all vectors are column vectors. Cauchy's formula gives the traction vector
 63 exerted on a fault plane by a stress as $\mathbf{t} = \boldsymbol{\sigma}\mathbf{n}$. The shear stress is derived by
 64 projecting \mathbf{t} onto fault plane as $\boldsymbol{\tau} = \mathbf{t} - \mathbf{n}\mathbf{n}^T\mathbf{t}$. The Wallace-Bott hypothesis
 65 requires $\boldsymbol{\tau}$ to be in the same direction as \mathbf{v} .

66 Fry (1999) decomposed the Wallace-Bott condition into

$$\mathbf{b} \cdot \mathbf{t} = 0 \quad (3)$$

67 and

$$\mathbf{v} \cdot \mathbf{t} > 0, \quad (4)$$

68 where the unit vector $\mathbf{b} = \mathbf{n} \times \mathbf{v}$ is perpendicular to both \mathbf{n} and \mathbf{v} . Eq. (3)
 69 requires the shear stress vector $\boldsymbol{\tau}$ to be parallel to observed slip direction \mathbf{v} ,
 70 while Eq. (4) represents the correspondence of shear sense (Fig. 2a). Sato
 71 and Yamaji (2006a) introduced the deviatoric stress space to stress inversion
 72 analysis, in which reduced stress tensors and fault-slip data are represented

73 by five-dimensional unit vectors (Fig. 2b). They reformulated Eqs. (3) and
 74 (4) as

$$\vec{\epsilon}' \cdot \vec{\sigma} = 0 \quad (5)$$

75 and

$$\vec{\epsilon} \cdot \vec{\sigma} > 0, \quad (6)$$

76 respectively. The vectors in Eqs. (5) and (6) are defined as

$$\vec{\sigma} = \begin{pmatrix} \sigma_{11}/\sqrt{2} \\ \sigma_{22}/\sqrt{2} \\ \sigma_{33}/\sqrt{2} \\ \sigma_{23} \\ \sigma_{31} \\ \sigma_{12} \end{pmatrix}, \quad \vec{\epsilon}' = \begin{pmatrix} \sqrt{2}b_1n_1 \\ \sqrt{2}b_2n_2 \\ \sqrt{2}b_2n_2 \\ b_2n_3 + b_3n_2 \\ b_3n_1 + b_1n_3 \\ b_1n_2 + b_2n_1 \end{pmatrix}, \quad \vec{\epsilon} = \begin{pmatrix} \sqrt{2}v_1n_1 \\ \sqrt{2}v_2n_2 \\ \sqrt{2}v_2n_2 \\ v_2n_3 + v_3n_2 \\ v_3n_1 + v_1n_3 \\ v_1n_2 + v_2n_1 \end{pmatrix}. \quad (7)$$

77 The normalisation conditions of the stress tensor (Eqs. 1 and 2) and the
 78 orthogonality of unit vectors representing fault parameters (Fig. 2a) imply

$$\sigma_{11} + \sigma_{22} + \sigma_{33} = \epsilon'_1 + \epsilon'_2 + \epsilon'_3 = \epsilon_1 + \epsilon_2 + \epsilon_3 = 0, \quad (8)$$

79

$$|\vec{\sigma}| = |\vec{\epsilon}'| = |\vec{\epsilon}| = 1, \quad (9)$$

80 and

$$\vec{\epsilon}' \cdot \vec{\epsilon} = 0. \quad (10)$$

81 Eq. (8) means the components of vectors in the direction of $(1, 1, 1, 0, 0, 0)^T$
 82 are equal to 0, which allows us to reduce the dimension on six-dimensional
 83 vectors to five. According to Eq. (9) the end points of vectors are on the
 84 five-dimensional unit sphere (Fig. 2b).

85 The Wallace-Bott condition is geometrically expressed in the deviatoric
86 stress space (Sato and Yamaji, 2006a). A fault-slip datum specifies paired
87 orthogonal vectors $\vec{\epsilon}'$ and $\vec{\epsilon}$ (Eq. 10). The unknown stress tensor is con-
88 strained so that $\vec{\sigma}$ is perpendicular to $\vec{\epsilon}'$ and is in the same hemisphere as
89 $\vec{\epsilon}$ (Eqs. 5 and 6). In other words, stress tensors which satisfy the Wallace-
90 Bott condition correspond to $\vec{\sigma}$ on a half great circle specified by $\vec{\epsilon}'$ and $\vec{\epsilon}$
91 (Fig. 2b), which is called the Fry arc in what follows.

92 *2.2. Analytical solution*

93 When we have a number of faults activated by a single stress, their Fry
94 arcs should intersect at a point on the five-dimensional unit sphere. The point
95 corresponds to the optimal stress tensor satisfying Wallace-Bott conditions
96 for all faults. Since natural data contain errors to some extent, intersections
97 of Fry arcs do not generally coincide. MIM searches for optimal points for
98 fault subsets which have small distances to Fry arcs. The candidates of
99 solutions are the uniformly spaced 60,000 grid points (Sato and Yamaji,
100 2006b). The exhaustive search on the grid causes the computational cost.

101 The necessary and sufficient number of fault data to determine a stress
102 solution is four, which is equal to the number of unknown stress parame-
103 ters. This fact corresponds to the geometry in the deviatoric stress space.
104 In order to satisfy the parallel conditions between shear stress vectors and
105 slip directions (Eq. 5) for four faults, a direction perpendicular to four $\vec{\epsilon}'$
106 vectors in the five-dimensional space is uniquely specified by calculating a
107 cross product of them (Fig. 3). Fortunately, the number of faults in a subset
108 of MIM analysis can be set to four. Then the time-consuming grid search
109 can be replaced by a direct calculation of cross product. The replacement

110 is expected to save computational time, although the shear sense conditions
111 (Eq. 6) must be checked separately.

112 2.3. Procedure

113 The present method of fast multiple inversion, hereafter FMI, takes the
114 following steps.

- 115 1. Convert N fault-slip data into $\vec{\epsilon}$ and $\vec{\epsilon}'$ vectors.
- 116 2. Extract a four-element subset from the whole data.
- 117 3. Calculate the five-dimensional cross product of four $\vec{\epsilon}'$ vectors to ob-
118 tain a candidate $\vec{\sigma}$ for the optimal solution.
- 119 4. Check the shear sense conditions (Eq. 6) by calculating dot products
120 of $\vec{\sigma}$ and $\vec{\epsilon}$ vectors. If all signs of four dot products are positive or
121 negative, $\vec{\sigma}$ or $-\vec{\sigma}$ is the optimal solution for the subset, respectively.
122 Otherwise, reject the candidate $\vec{\sigma}$ and proceed to 6.
- 123 5. Find the nearest grid point to the optimal solution from 60,000 uniform
124 grid points and cast a vote for the corresponding stress tensor.
- 125 6. Repeat procedures 2 to 5 ${}_N C_4$ times for all possible combinations of
126 fault subsets.

127 The software of FMI is available at the author's web site ([http://www.kueps.kyoto-](http://www.kueps.kyoto-u.ac.jp/~web-bs/k_sato/software.html)
128 [u.ac.jp/~web-bs/k_sato/software.html](http://www.kueps.kyoto-u.ac.jp/~web-bs/k_sato/software.html)).

129 Step 5 above is necessary to deal with numerous stress tensors. When
130 $N = 100$, for example, we need to find concentrations of ${}_{100}C_4 = 3,921,225$
131 solutions, though step 4 probably reduces the number to some extent. The
132 population of solutions are converted into votes for grid points. The peaks

133 of distribution of votes on the five-dimensional unit sphere can be visualised
134 and recognised by viewer software.

135 Noisy votes in the result of MIM analysis partly comes from heterogeneous
136 fault subsets, for which the optimal solutions are meaningless and expected
137 to be random stress tensors (Yamaji, 2000). Otsubo and Yamaji (2006)
138 proposed a method to reduce such noise by excluding a candidate solution
139 if the distance between corresponding $\vec{\sigma}$ vector and at least one Fry arc is
140 larger than a threshold value. In the present method of FMI step 4 performs
141 the exclusion during the check of shear sense conditions.

142 Another type of noise can arise from the instability of cross product cal-
143 culated in step 3. If four $\vec{\epsilon}'$ vectors are not sufficiently linearly independent,
144 i.e., at least two of them are nearly parallel, the direction of their cross prod-
145 uct becomes instable. The degree of linear independence is measured by the
146 length of the cross product, which is the volume of four-dimensional paral-
147 lelepiped spanned by $\vec{\epsilon}'$ vectors. The length ranges from 0 to 1. For the
148 purpose of reducing noisy votes, FMI has an option to weight votes propor-
149 tionally to the lengths of cross products in the procedure 5.

150 **3. Improvement**

151 *3.1. Test 1: Reduction of calculation time*

152 Artificial fault-slip data sets were analysed to compare the calculation
153 times of MIM and FMI. The number of faults in a subset k in MIM was
154 set to four. An example of a data set is shown in Fig. 4a. Fault planes
155 are randomly oriented. A half of the faults in a data set is assumed to be
156 activated by stress A with σ_1 -axis at 000/00, σ_3 -axis at 090/00 and $\Phi = 0.3$.

157 The other half corresponds to stress B with σ_1 -axis at 040/00, σ_3 -axis at
158 130/00 and $\Phi = 0.3$. The parameter $\Phi = (\sigma_2 - \sigma_3) / (\sigma_1 - \sigma_3)$ is called stress
159 ratio, which ranges from 0 to 1. $\Phi = 0$ for axial compression ($\sigma_1 > \sigma_2 = \sigma_3$)
160 and $\Phi = 1$ for axial tension ($\sigma_1 = \sigma_2 > \sigma_3$).

161 As the result of MIM and FMI analyses, the artificial stresses A and B
162 were successfully detected (Fig. 4b and c). No large difference was found
163 between results of MIM with grid search and FMI with direct calculation
164 as is expected. The time spent for calculation is shown in Fig. 5a for the
165 cases of $N = 50$ to 500. Although the calculation time rapidly increases with
166 the number of data for both methods, FMI was found to be about ten times
167 faster than MIM.

168 The calculation time for analysis of seismic focal mechanisms was also
169 examined (Fig. 5b). For a four-element subset, the number of possible
170 choices between orthogonal nodal planes is $2^4 = 16$. All choices are regarded
171 as different subsets of faults in both MIM and FMI, of which calculation
172 inevitably requires much longer time than analysis of geological fault data.
173 Fig. 5b clearly shows that FMI is several times faster than MIM.

174 *3.2. Test 2: Noise reduction*

175 As is mentioned in Section 2.3, FMI has an option to reduce noisy so-
176 lutions by weighting them according to the lengths of five-dimensional cross
177 products. This option can reduce noises caused by nearly parallel $\vec{\epsilon}'$ vectors
178 which correspond to nearly parallel fault planes and slip directions. In order
179 to test the effect of noise reduction, an artificial fault data set with 100 faults
180 were analysed (Fig. 6). The faults were assumed to be activated by a single
181 stress tensor with stress ratio Φ of 0.3 and with σ_1 - and σ_3 -axes oriented

182 340/10 and 160/80, respectively. The normals of fault planes were concen-
183 trated at 000/45 and 180/45 with some perturbation, simulating a conjugate
184 fault system.

185 As the results of MIM (Fig. 6b), FMI (Fig. 6c) and FMI with noise
186 reduction (Fig. 6d), the assumed stress tensor was successfully detected.
187 The difference between methods appeared in the accuracy and precision of
188 solution. The accuracy can be measured by angular stress distance Θ (Yamaji
189 and Sato, 2006), which is the reformulation of stress difference proposed by
190 Orife and Lisle (2003), between optimal solutions and the assumed stress
191 tensor. MIM resulted in $\Theta = 5.38^\circ$, while FMI with noise reduction had a
192 higher accuracy of $\Theta = 1.61^\circ$. The precision was measured by the dispersion
193 of numerous solutions derived from all fault subsets, which can be estimated
194 by the mean distance $\bar{\Theta}$ to the optimal (averaged) solution. FMI with noise
195 reduction was found to have higher precision of $\bar{\Theta} = 15.6^\circ$ than that of MIM,
196 $\bar{\Theta} = 22.7^\circ$. The weighting of solutions by the lengths of cross products was
197 confirmed to be effective in reducing noise.

198 4. Discussion

199 The new method of multiple stress inversion (FMI) was found to accel-
200 erate the calculation by a factor of up to 10 without loss of detectability of
201 stress tensors. Moreover, the noise reduction technique is available in FMI
202 analysis. However, the dependence of calculation amount of FMI on the
203 number of fault data is still $O(N^4)$, the same as MIM, as is demonstrated by
204 the rapidly increasing trends of calculation time in Fig. 5. It will take several
205 days to analyse more than a thousand faults by using personal computers.

206 The problem is severe especially for seismic focal mechanisms because of the
207 availability of databases accumulating numerous seismic events and the un-
208 known choice between nodal planes. Further reduction of calculation time
209 could be achieved by relaxing the requirement of analysing all possible com-
210 binations of fault subsets. We could undertake random sampling of fault
211 subsets to limit the computation effort, which of course requires a careful
212 assessment of degeneration of results.

213 **Acknowledgement**

214 The author is grateful to Dr. R.J. Lisle and Dr. T.G. Blenkinsop for
215 their detailed reviews and suggestions which improved the manuscript. This
216 work was partly supported by JSPS KAKENHI 21740364.

217 **References**

- 218 Angelier, J., 1979. Determination of the mean principal directions of stresses
219 for a given fault population. *Tectonophysics* 56 (3-4), T17–T26.
- 220 Bott, M.H.P., 1959. The mechanics of oblique slip faulting. *Geological Mag-*
221 *azine* 96 (2), 109–117.
- 222 Chan, L.S., Shen, W., Pubellier, M., 2010. Polyphase rifting of greater Pearl
223 River Delta region (South China): Evidence for possible rapid changes in
224 regional stress configuration. *Journal of Structural Geology* 32 (6), 746 –
225 754.
- 226 Fry, N., 1999. Striated faults: visual appreciation of their constraint on pos-
227 sible paleostress tensors. *Journal of Structural Geology* 21 (1), 7–21.

- 228 Orife, T., Lisle, R.J., 2003. Numerical processing of palaeostress results. Jour-
229 nal of Structural Geology 25 (6), 949–957.
- 230 Otsubo, M., Yamaji, A., 2006. Improved resolution of the multiple inverse
231 method by eliminating erroneous solutions. Computers & Geosciences
232 32 (8), 1221–1227.
- 233 Otsubo, M., Yamaji, A., Kubo, A., 2008. Determination of stresses from
234 heterogeneous focal mechanism data: An adaptation of the multiple inverse
235 method. Tectonophysics 457 (3-4), 150–160.
- 236 Sato, K., Yamaji, A., 2006a. Embedding stress difference in parameter space
237 for stress tensor inversion. Journal of Structural Geology 28 (6), 957–971.
- 238 Sato, K., Yamaji, A., 2006b. Uniform distribution of points on a hypersphere
239 for improving the resolution of stress tensor inversion. Journal of Structural
240 Geology 28 (6), 972–979.
- 241 Sippel, J., Scheck-Wenderoth, M., Reicherter, K., Mazur, S., 2009. Pale-
242 ostress states at the south-western margin of the Central European Basin
243 System – Application of fault-slip analysis to unravel a polyphase defor-
244 mation pattern. Tectonophysics 470 (1-2), 129 – 146.
- 245 Twiss, R.J., Gefell, M.J., 1990. Curved slickenfibers - a new brittle shear sense
246 indicator with application to a sheared serpentinite. Journal of Structural
247 Geology 12 (4), 471–481.
- 248 Wallace, R.E., 1951. Geometry of shearing stress and relation to faulting.
249 Journal of Geology 59 (2), 118–130.

- 250 Yamada, Y., Yamaji, A., 2002. Determination of palaeostresses from
251 mesoscale shear fractures in core samples using the multi-inverse method.
252 *Journal of Petroleum Geology* 25 (2), 203–218.
- 253 Yamaji, A., 2000. The multiple inverse method: a new technique to separate
254 stresses from heterogeneous fault-slip data. *Journal of Structural Geology*
255 22 (4), 441–452.
- 256 Yamaji, A., 2003. Slab rollback suggested by latest Miocene to Pliocene
257 forearc stress and migration of volcanic front in southern Kyushu, northern
258 Ryukyu arc. *Tectonophysics* 364 (1-2), 9–24.
- 259 Yamaji, A., Sato, K., 2006. Distances for the solutions of stress tensor inver-
260 sion in relation to misfit angles that accompany the solutions. *Geophysical*
261 *Journal International* 167 (2), 933–942.
- 262 Yamaji, A., Sato, K., 2011. A spherical code and stress tensor inversion.
263 *Computers & Geosciences*, in press.

264 **Figure captions**

265 *Figure 1*

266 Schematic figure illustrating the procedure of multiple inverse method
267 (MIM) to detect multiple stress tensors from a heterogeneous fault-slip data
268 set. The data set is a mixture of black and white f symbols representing faults
269 activated by different stresses A and B, respectively. MIM extracts subsets
270 of four or five faults from whole data and determines optimal solutions for
271 them by means of exhaustive grid search on the deviatoric stress space (Sato
272 and Yamaji, 2006b) which is geometrically the surface of five-dimensional
273 unit sphere. Homogeneous subsets are expected to concentrate their votes
274 to the grid points corresponding to stresses A or B, while the meaningless
275 solutions from heterogeneous subsets should be placed randomly.

276 *Figure 2*

277 Wallace-Bott hypothesis as the principle of stress tensor inversion. The
278 slip direction of a fault is assumed to coincide with the shear stress direction
279 exerted by the tectonic stress in question. (a) In the physical space, observ-
280 able fault parameters are represented by unit vectors \mathbf{v} , \mathbf{b} and \mathbf{n} . A correct
281 stress tensor gives shear stress vector $\boldsymbol{\tau}$, which is the projection of traction
282 vector \mathbf{t} onto fault plane, in the direction of slip \mathbf{v} . (b) Schematic figure of
283 deviatoric stress space. Wallace-Bott hypothesis is geometrically expressed
284 as the constraint on stress tensor represented by $\vec{\sigma}$ from a fault-slip datum.
285 The fault parameters $\vec{\epsilon}$ and $\vec{\epsilon}'$ specify a half great circle called the Fry arc
286 (bold line) on which $\vec{\sigma}$ vector is required to lie.

287 *Figure 3*

288 Schematic figure illustrating how to calculate the direct solution of stress
289 tensor inversion. When we have four fault-slip data, four $\vec{\epsilon}'$ vectors are
290 specified in the five-dimensional deviatoric stress space. The parallel condi-
291 tions between fault-slip directions and shear stress vectors require $\vec{\sigma}$ vector
292 representing stress tensor to be perpendicular to all four $\vec{\epsilon}'$ vectors. The an-
293 alytical solution to this even-determined problem can be uniquely obtained
294 as the direction of five-dimensional cross product of $\vec{\epsilon}'$ vectors. Note that
295 four $\vec{\epsilon}'$ vectors must be linearly independent in the five-dimensional space,
296 although this schematic figure looks as if they were two-dimensionally copla-
297 nar owing to lack of dimension. The white circle spanned by them represents
298 not a two-dimensional circle but a four-dimensional space.

299 *Figure 4*

300 An example of results of the test to examine the computational cost of
301 FMI. (a) Artificial fault-slip data containing 50 faults of which half is acti-
302 vated by stress A and the other half is activated by stress B. Tangent-lineation
303 diagram (Twiss and Gefell, 1990) in lower-hemisphere and equal-area pro-
304 jection. Arrows plotted at poles of fault planes indicate slip directions of
305 footwall blocks. (b) Result of MIM. Paired stereograms show orientations of
306 σ_1 - and σ_3 -axes. Colours of symbols indicate stress ratio Φ . In this figure
307 300 stress tensors out of 60,000 grid points are plotted, which got more votes
308 from fault subsets than the others. The assumed stresses A and B were cor-
309 rectly detected. (c) Result of FMI in similar plot as (b). Note that there is
310 no significant difference between results of MIM and FMI.

311 *Figure 5*

312 Comparison of calculation times of MIM and FMI. Horizontal axis is the
313 number of faults analysed. (a) Analysis of geological faults. FMI works about
314 ten times faster than MIM, although the calculation times of both methods
315 increase rapidly with the number of data. (b) FMI is also faster in analysis
316 of seismic focal mechanisms, although they require much longer time than
317 geological faults because of unknown choice of nodal planes.

318 *Figure 6*

319 The result of analysis to test the effect of noise reduction. (a) Artificial
320 100 fault-slip data assumed to be activated by a single stress with $\Phi = 0.3$.
321 Open squares are principal stress axes plotted on lower-hemisphere and equal-
322 area stereogram. Arrows show the slip directions of footwall blocks plotted
323 at poles of fault planes (tangent-lineation diagram). (b) Result of MIM.
324 (c) Result of FMI. (d) Result of FMI with noise reduction. See Fig. 4
325 for explanation of plots. Φ values show stress ratios of optimal solutions of
326 which principal orientations are plotted as open squares. The accuracies of
327 the optimal solutions were measured by Θ values which are distances from the
328 assumed stress. $\bar{\Theta}$ is the dispersion of solutions obtained from fault subsets
329 as a measure of precision. Stress tensors of which votes are more than 1.5%
330 of their maximum are plotted. Note that higher accuracy and precision was
331 achieved by noise reduction in FMI.

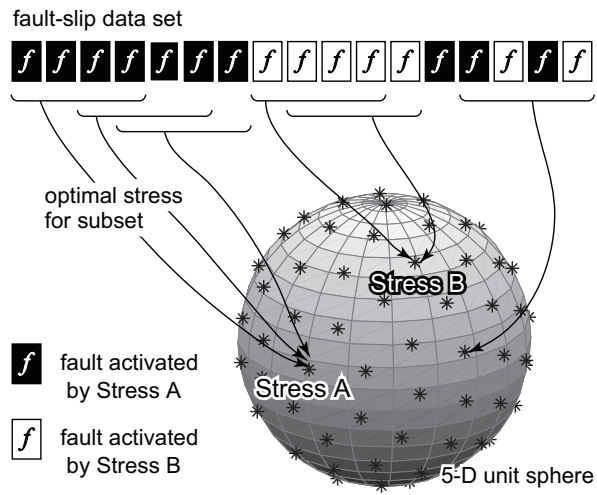


Figure 1: Sato.

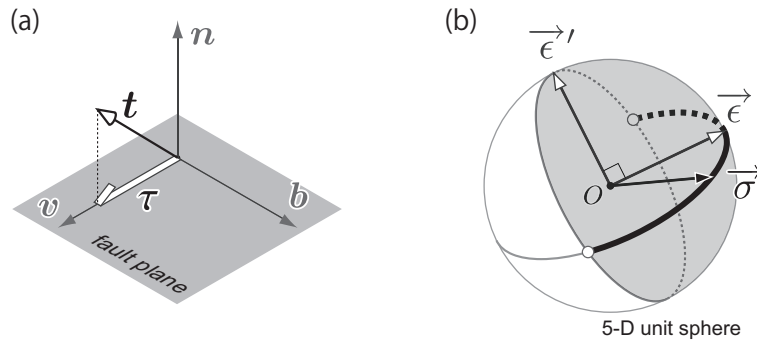


Figure 2: Sato.

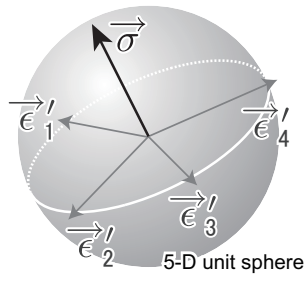


Figure 3: Sato.

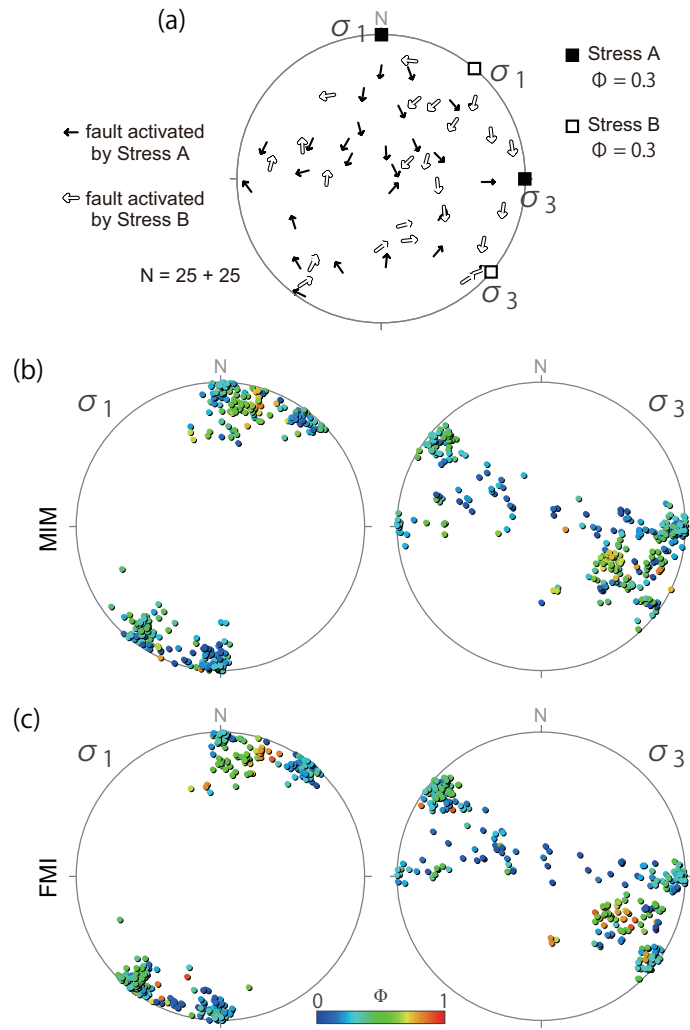


Figure 4: Sato.

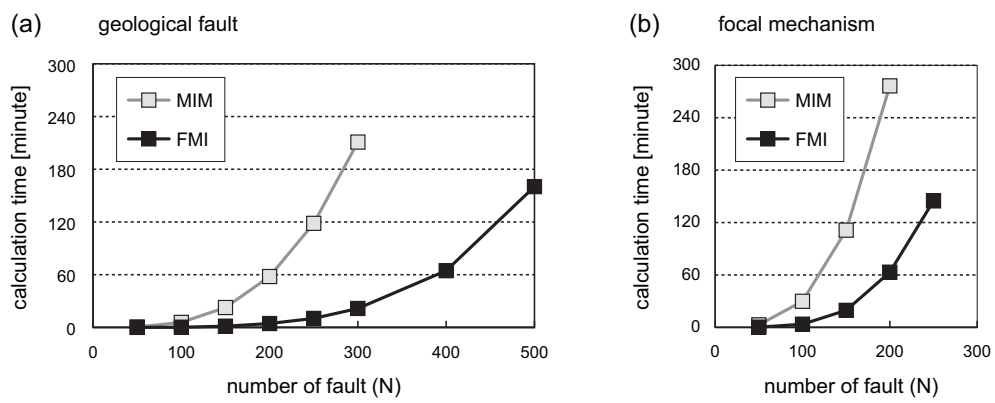


Figure 5: Sato.

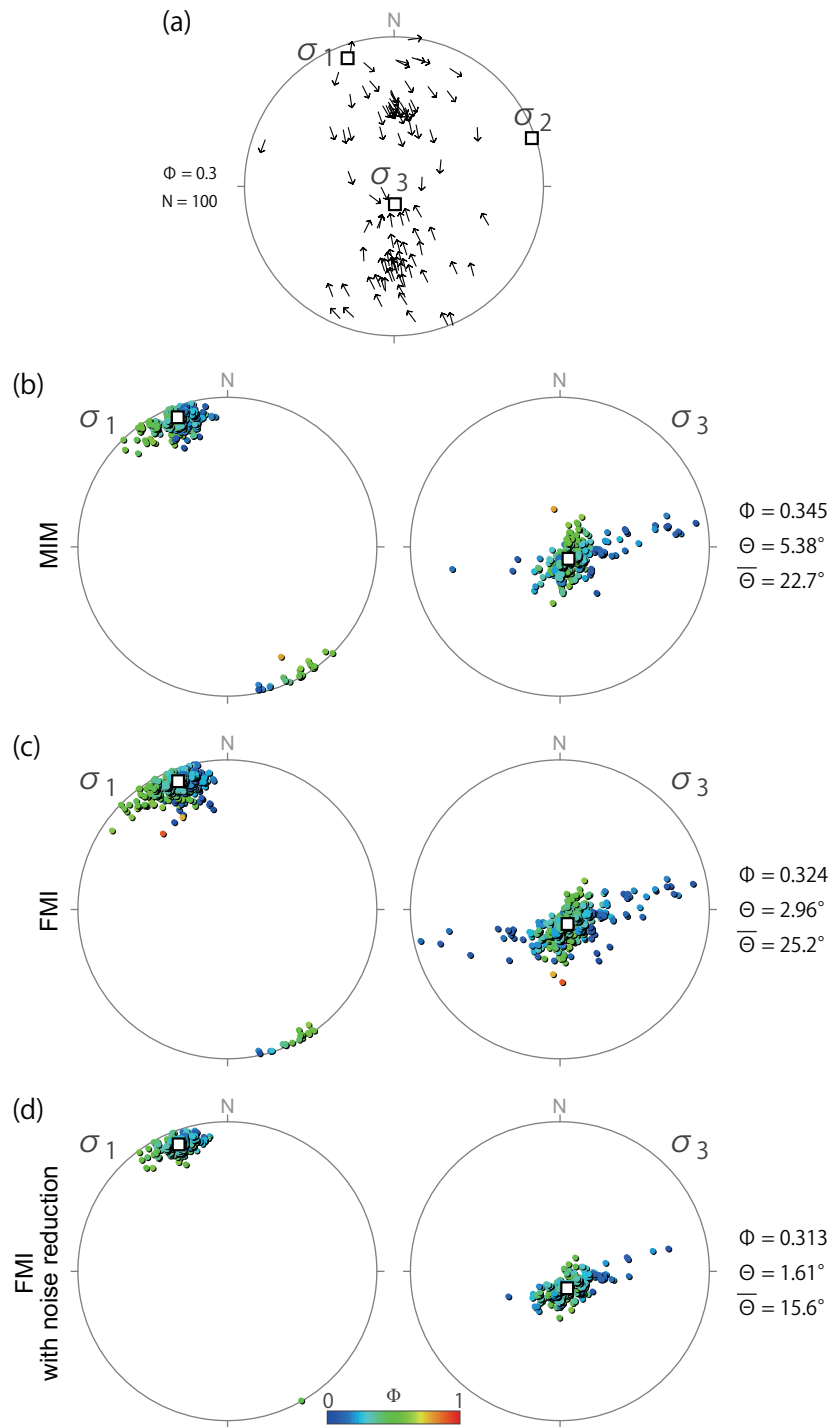


Figure 6: Sato.